Sensors and Materials, Vol. 34, No. 2 (2022) 575–583
MYU Tokyo

S & M 2829

Scintillation Properties of an Organic–Inorganic Lead Iodide Perovskite Single Crystal Having Quantum Well Structures

Kai Okazaki,[1*] Daichi Onoda,[1] Daisuke Nakauchi,[1] Naoki Kawano,[2]
Hiroyuki Fukushima,[1] Takumi Kato,[1] Noriaki Kawaguchi,[1] and Takayuki Yanagida[1]

[1]Division of Materials Science, Nara Institute of Science and Technology (NAIST),
8916-5 Takayama-Cho Ikoma, Nara 630-0192, Japan
[2]Graduate School of Engineering Science, Akita University,
1-1 Tegatagakuen-machi, Akita City, Akita 010-8502, Japan

(Received October 5, 2021; accepted October 27, 2021)

Keywords: organic–inorganic perovskite compound, quantum well structure, lead iodide, scintillator, photoluminescence

A $(C_6H_5C_2H_4NH_3)_2PbI_4$ crystal was prepared to investigate its photoluminescence (PL) and scintillation properties. Two PL emission peaks at 525 and 560 nm derived from the recombination of excitons were observed. The obtained PL decay curve was approximated from the sum of three exponential decay functions related to the excitonic luminescence. Under X-ray irradiation, the excitonic emission at 560 nm from shallow trap centers was observed, and the X-ray induced scintillation decay times were 0.8, 6.0, and 37 ns. The full energy peak was observed under ^{241}Am α-ray (5.5 MeV) irradiation, and the light yield was estimated to be ~2900 ph/5.5 MeV-α.

1. Introduction

Scintillators are a type of phosphor that immediately converts ionizing radiation into low-energy photons in UV-NIR regions.[1–3] Scintillation detectors are mainly composed of scintillators and photodetectors,[4] and ionizing radiation can be detected as electric signals since scintillation photons are converted into electrons through photodetectors. For X- and γ-ray detector uses, the following properties are generally required: high light yields (*LY*), large effective atomic number (Z_{eff}), high density, short scintillation decay time, low afterglow, and low fabrication costs.[5,6] Applications of scintillators cover wide fields such as medical imaging,[7] space explorations,[8] well logging,[9] and inspection equipment for security.[10] The required properties are varied. For instance, positron emission tomography (PET) is a type of medical diagnosis imaging technique, especially for cancer diagnosis. In PET, scintillation detectors arranged in a circle around a human body simultaneously detect two γ-rays (511 keV) emitted in opposite directions. Owing to the characteristics of the measurements, sufficient energy resolution to distinguish 511 keV γ-rays from scattered signals, high detection efficiency, and high time resolution are important. Therefore, inorganic scintillators having large Z_{eff} and

*Corresponding author: e-mail: okazaki.kai.of0@ms.naist.jp
https://doi.org/10.18494/SAM3678

ISSN 0914-4935

fast decay time, such as Tl:NaI (Z_{eff} ~51), $Bi_4Ge_3O_{12}$ (Z_{eff} ~75), Ce:Gd_2SiO_5 (Z_{eff} ~59), and Ce:Lu_2SiO_5 (LSO, Z_{eff} ~66), were historically employed in PET.[11–13] However, with the progress of techniques such as the invention of time-of-flight PET/computed tomography[14,15] and positron emission mammography,[16] higher performance, especially high *LY* with fast decay time, has been required for scintillators.

Two-dimensional (2D) organic–inorganic hybrid perovskite-type compounds, which are a type of semiconductor scintillator, have recently attracted considerable attention and have been expected to achieve the above requirements. This type of material has quantum well structures that can confine excitons.[17] The structures consist of organic layers as barriers and inorganic layers as wells, since the organic layers have a higher bandgap energy than the inorganic layers. Excitons confined in the inorganic layers have a high binding energy, and thus fast and highly efficient luminescence can be expected.[18,19] As further advantages, the perovskite crystals can be grown at a low cost owing to a low-temperature process in comparison with most inorganic scintillators synthesized by melt-growth methods (e.g., Czochralski, Bridgeman, and Floating Zone methods).[6,20–22] According to a previous study, $(C_6H_5C_2H_4NH_3)_2PbBr_4$ has shown high *LY* (14000 ph/MeV) and fast scintillation decay time (11 ns).[23] On the basis of this study, various types of lead bromide-based organic–inorganic hybrid perovskite-type compounds have been continuously explored,[24–28] whereas there have been only a few reports on the scintillation properties of other halide-based organic–inorganic hybrid perovskite-type compounds (e.g., lead chloride- and iodide-based ones). In a previous report on the lead iodide-based one, extremely fast scintillation decay times were reported on (n-$C_6H_{13}NH_3)_2PbI_4$ (390 ps).[29] Therefore, lead iodide-based compounds can be expected as fast-response scintillators. Furthermore, lead iodide-based compounds are considered to have an advantage for X- and γ-ray detection since iodide has a larger Z_{eff} (~61) than bromide (Z_{eff} ~60). In this study, we prepared a $(C_6H_5C_2H_4NH_3)_2PbI_4$ crystal, a type of lead iodide-based organic–inorganic hybrid perovskite-type compound, and its photoluminescence (PL) and scintillation properties were investigated.

2. Materials and Methods

2.1 Materials preparation

A $(C_6H_5C_2H_4NH_3)_2PbI_4$ single crystal was grown by the slow-cooling method. First, the precursor of the organic layer was prepared. $C_6H_5C_2H_4NH_2$ (2-phenylethylamine, 99%, Alfa Aesar) and HI (55–58%, Wako Pure Chemical Industries, 1 equiv.) were stirred at room temperature in *N, N*-dimethylformamide (DMF, 99.5%, Wako Pure Chemical Industries) solvent. Subsequently, the solvent was evaporated to obtain $C_6H_5C_2H_4NH_3I$ powder, and then the powder was stirred with PbI_2 (99.99%, High Purity Chemicals, 0.5 equiv.) in DMF. The $(C_6H_5C_2H_4NH_3)_2PbI_4$ powder was obtained by evaporating the solvent. After that, the obtained $(C_6H_5C_2H_4NH_3)_2PbI_4$ powder was dissolved into the mixed solvent of DMF and CH_3NO_2 (96%, Wako Pure Chemical Industries) at 90 °C with stirring. Finally, the solution was gradually cooled from 90 to 20 °C at the rate of 3.5 °C/h using a liquid phase synthesizer (Chemi Chemi-300, Shibata) to obtain a $(C_6H_5C_2H_4NH_3)_2PbI_4$ single crystal.

2.2 Experimental setup

The crystalline structure was investigated by measuring the powder X-ray diffraction (XRD) patterns with a diffractometer (MiniFlex600, Rigaku). The tested range of the diffraction angle (2θ) was 3–50°. The diffuse transmission spectrum was measured with a spectrophotometer (SolidSpec-3700, Shimadzu).

The PL excitation spectra were measured with a spectrofluorometer (FP-8600, JASCO). A band-pass filter (HMX0530, AsahiSpectra) and short-cut filter (LV0510, AsahiSpectra) were used to measure the excitation spectrum monitored at 525 nm, and a band-pass filter (HMX0570, AsahiSpectra) and short-cut filter (LV0570, AsahiSpectra) were used to measure the excitation spectrum monitored at 560 nm. The PL emission spectrum and PL decay curve were measured using a Quantaurus-τ (C11367, Hamamatsu Photonics). A Quantaurus-QY (C11347, Hamamatsu Photonics) was used for quantum yield (*QY*) measurement. The scintillation properties were investigated by measuring the following: X-ray-induced scintillation spectrum, X-ray-induced scintillation decay curve, afterglow curve, and pulse-height spectrum using our original setups.[30,31]

3. Results and Discussion

A photograph of the prepared $(C_6H_5C_2H_4NH_3)_2PbI_4$ single crystal is shown in Fig. 1. The diameter and thickness were around 5 mm and 0.28 mm, respectively. The appearance was orangish transparent owing to band-edge absorption in the inorganic layers.

Figure 2 shows the XRD pattern of the $(C_6H_5C_2H_4NH_3)_2PbI_4$ single crystal. Diffraction peaks were observed at a regular interval. The peaks corresponded to (0 0 2l) planes (l = 1, 2, 3, 4, 5, 6), and the present result indicated that this sample has the 2D quantum well structures.[23] The lattice constant of the c-axis was estimated to be ~16.3 Å, which was almost the same as that

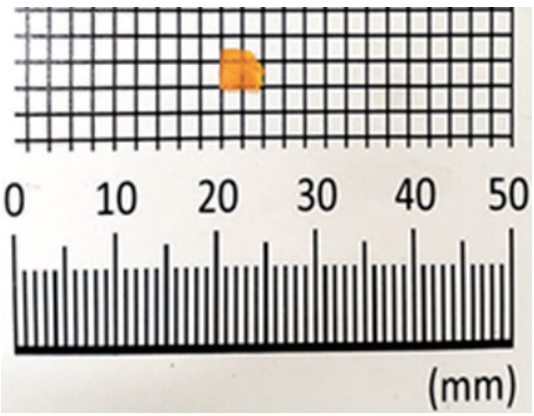

Fig. 1. (Color online) Photograph of $(C_6H_5C_2H_4NH_3)_2PbI_4$ single crystal.

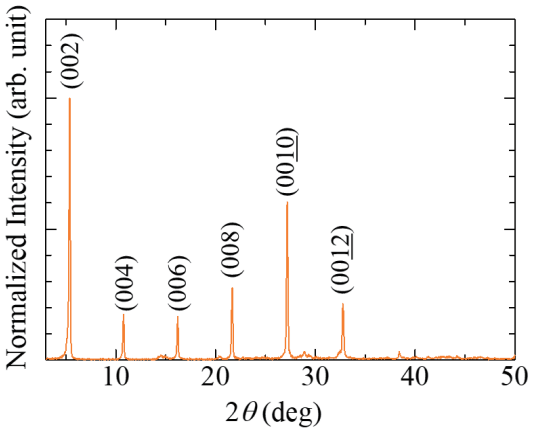

Fig. 2. (Color online) X-ray diffraction pattern of $(C_6H_5C_2H_4NH_3)_2PbI_4$ single crystal.

of $(C_6H_5C_2H_4NH_3)_2PbBr_4$ (~16.4 Å[23]). In addition, some weak diffraction peaks were observed. The diffraction peaks were not attributable to raw materials such as $C_6H_5C_2H_4NH_3I$ and PbI_2.[32] The $(C_6H_5C_2H_4NH_3)_2PbI_4$ reported in the previous study shows almost the same pattern, including the weak peaks due to crystal planes other than (0 0 2*l*),[33] which demonstrated the low crystal quality of the sample in this study.

Figure 3 shows the diffuse transmission spectrum of the $(C_6H_5C_2H_4NH_3)_2PbI_4$ single crystal. The absorption band due to the electronic transition from Pb(6s)-I(5p) to Pb(6p)[34] was observed at wavelengths shorter than 540 nm, which is consistent with the optical bandgap energy (2.57 eV) of $(C_6H_5C_2H_4NH_3)_2PbI_4$ reported in a previous study.[35] The transmittance was 50–70% at wavelengths longer than 540 nm.

Figure 4 shows the PL excitation and emission spectra of the $(C_6H_5C_2H_4NH_3)_2PbI_4$ single crystal. The PL emission peaks were observed under the excitation light at 470 nm. Double emission peaks were observed at 525 and 560 nm. The peak at 525 nm was derived from the recombination of free excitons,[36] and the peak at 560 nm originated from the recombination of excitons at the shallow trap centers.[37] The *QY* was lower than 1% in the range of 500–600 nm upon excitation at 510 nm. The excitation peak monitored at 525 or 560 nm was observed at 470 and 490 nm. Since the spectral shape was similar to those in $(n\text{-}C_6H_{13}NH_3)_2PbI_4$,[17,38] the origins of the signals at 470 and 490 nm were the bandgap in inorganic layers and the exciton absorption, respectively. The difference in spectral shapes depending on the excitation wavelengths was due to the difference in the optical filters used.

The PL decay curve of the $(C_6H_5C_2H_4NH_3)_2PbI_4$ single crystal and the instrumental response function (IRF) are shown in Fig. 5 The excitation and emission wavelengths were 470 and 525 nm, respectively. The decay curve was approximated from the sum of three exponential decay functions. The first component (0.7 ns) was derived from the recombination of free excitons confined in inorganic layers.[37] The second (1.6 ns) and third (15 ns) components were comparable to those of other lead iodide-based perovskites;[29] therefore, they were considered to

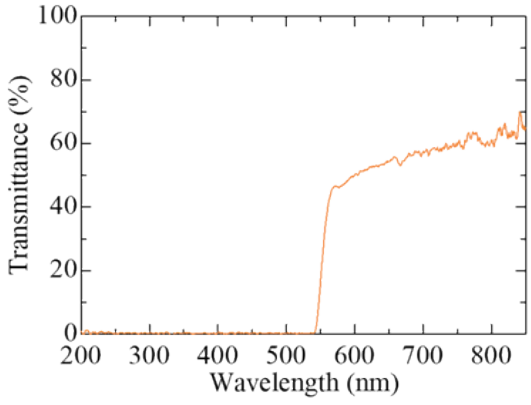

Fig. 3. (Color online) Diffuse transmission spectrum of $(C_6H_5C_2H_4NH_3)_2PbI_4$ single crystal.

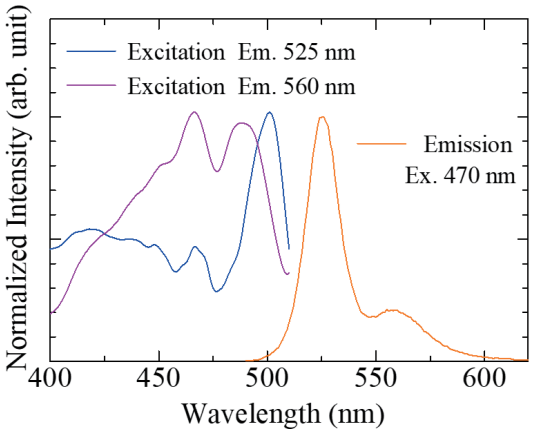

Fig. 4. (Color online) PL excitation/emission spectra of $(C_6H_5C_2H_4NH_3)_2PbI_4$ single crystal.

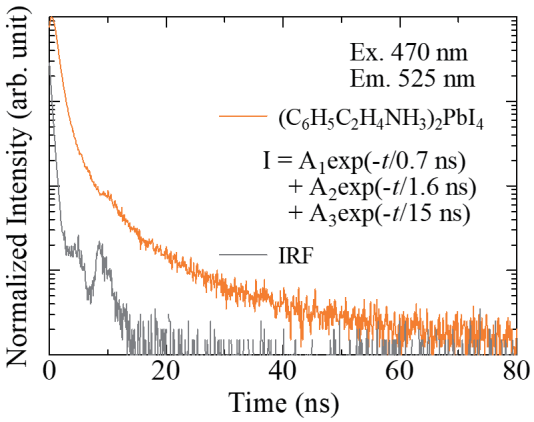

Fig. 5. (Color online) PL decay curve of $(C_6H_5C_2H_4NH_3)_2PbI_4$ single crystal.

be derived from the recombination of excitons at the shallow trap centers, which was also observed in $(n\text{-}C_6H_{13}NH_3)_2PbI_4$.[29]

Figure 6 shows the X-ray-induced scintillation spectrum. The observed peak at 560 nm was originated from the recombination of excitons at the shallow trap centers.[39] The peak at 525 nm observed in the PL spectrum was not observed owing to self-absorption.[40] The emission peak was longer than that of the $(C_6H_5C_2H_4NH_3)_2PbBr_4$ single crystal observed at 437 nm.[23] It can be considered that the lead iodide-based compounds have the low-energy bandgap in inorganic layers in comparison with the lead bromide-based compounds. In general, the excitonic luminescence of semiconductor scintillators is difficult to clearly observe owing to thermal quenching at room temperature.[41] On the other hand, the peak clearly appeared in the present sample even at room temperature, which was due to the quantum confinement effect.[42]

Figure 7 shows the X-ray-induced scintillation decay curve. The obtained decay curve was approximated from the sum of three exponential decay functions, similarly to the PL. The first component (0.8 ns) was attributed to the recombination of free excitons. The decay time constant of IRF was 0.5 ns; thus, the first component could be distinguished from IRF. The second (6.0 ns) and third (37 ns) components were considered to be derived from the recombination of excitons at the shallow trap centers like in PL.[29] The decay time constants were long in comparison with the PL decay time constants because of the differences in the mechanism between scintillation and PL; scintillation includes additional processes such as conversion and transfer processes compared with PL, and thus the present result is reasonable. The decay time of the first component (0.8 ns) was much faster than that of LSO (40 ns[11]), which is the conventional scintillator for PET. Moreover, the value was faster than that of the $(C_6H_5C_2H_4NH_3)_2PbBr_4$ (11 ns).

The pulse height spectrum measured using the $(C_6H_5C_2H_4NH_3)_2PbI_4$ single crystal is shown in Fig. 8. The figure includes a spectrum of ^{137}Cs γ-rays (0.662 MeV) measured with a Ce:$Y_3Al_5O_{12}$ (YAG) ceramic as a reference with *LY* of 20000 ph/MeV.[43] The $(C_6H_5C_2H_4NH_3)_2PbI_4$ single crystal did not show a photoabsorption peak under ^{137}Cs γ-ray irradiation owing to its low crystallinity; thus, ^{241}Am α-ray (5.5 MeV) was used as a radiation source. Under α-ray

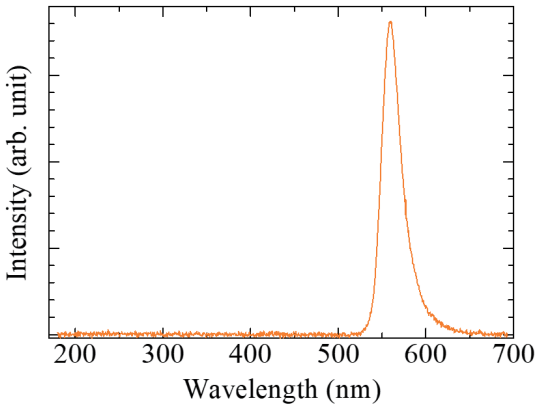

Fig. 6. (Color online) X-ray-induced scintillation spectrum of $(C_6H_5C_2H_4NH_3)_2PbI_4$ single crystal.

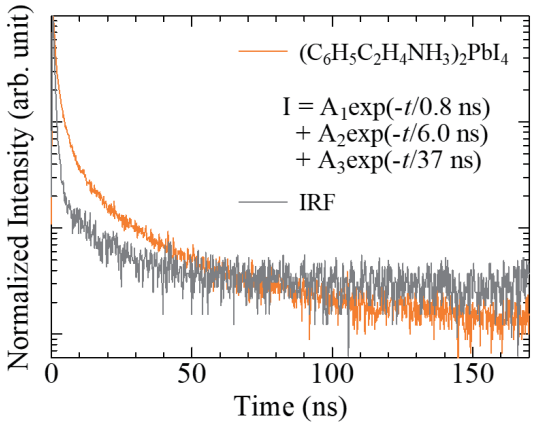

Fig. 7. (Color online) X-ray-induced scintillation decay curve of $(C_6H_5C_2H_4NH_3)_2PbI_4$ single crystal.

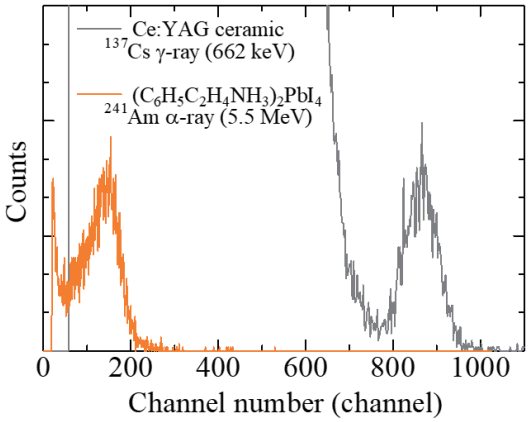

Fig. 8. (Color online) Pulse height spectrum of ^{241}Am α-rays measured using $(C_6H_5C_2H_4NH_3)_2PbI_4$ single crystal and that of ^{137}Cs γ-rays measured using Ce:YAG ceramic.

irradiation, a clear full energy absorption peak of the $(C_6H_5C_2H_4NH_3)_2PbI_4$ single crystal was observed at 190 channels, whereas that of the YAG ceramic was observed at 880 channels. Comparing the channels of the photoabsorption and full-energy peaks, we estimated the *LY* of the $(C_6H_5C_2H_4NH_3)_2PbI_4$ single crystal to be ~2,900 ph/5.5 MeV-α. The *LY* was lower than that of the $(C_6H_5C_2H_4NH_3)_2PbBr_4$ single crystal (~14000 ph/MeV) measured under ^{137}Cs γ-ray irradiation. However, under ^{241}Am α-rays, the *LY* of the $(C_6H_5C_2H_4NH_3)_2PbI_4$ was higher than those of ZnO in single crystal (~500 ph/5.5 MeV-α)[44] and ceramic (~1500 ph/5.5 MeV-α) forms,[45] a type of semiconductor scintillator.

Figure 9 shows the afterglow curve of the $(C_6H_5C_2H_4NH_3)_2PbI_4$ single crystal. The afterglow level (A) was defined using the formula $A = (I_{20} - I_{BG})/ (I_{MAX} - I_{BG})$. I_{20}, I_{BG}, and I_{MAX} are the emission intensity 20 ms after X-ray cut off, the background intensity before X-ray irradiation, and the emission intensity during X-ray irradiation, respectively. The calculated A was 39.8 ppm.

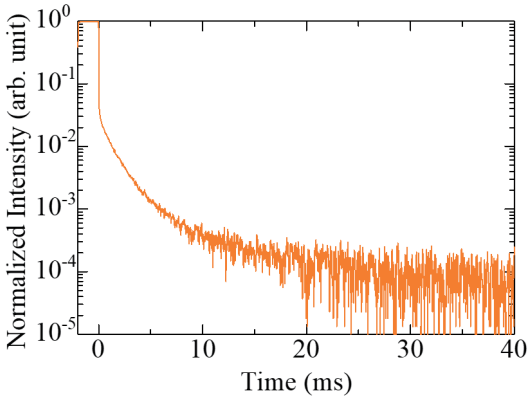

Fig. 9. (Color online) Afterglow curve of $(C_6H_5C_2H_4NH_3)_2PbI_4$ single crystal under X-ray exposure.

This value is worse than that of the $(C_6H_5C_2H_4NH_3)_2PbBr_4$ (5 ppm[23]). However, it is much better than that of Tl:CsI (268 ppm[46]), which is a commercialized scintillator for security inspection.

4. Conclusions

The $(C_6H_5C_2H_4NH_3)_2PbI_4$ single crystal, a type of organic–inorganic hybrid perovskite-type compound, was prepared by the slow-cooling method. In PL and scintillation spectra, the excitonic luminescence was observed. The PL and scintillation decay curves were approximated from the sum of three exponential decay functions due to excitonic luminescence. The scintillation decay time (0.8 ns) related to the free-exciton luminescence was much faster than those of the conventional scintillators for PET. The *LY* was 2,900 ph/5.5 MeV-α, which was higher than those of ZnO in single crystal (500 ph/5.5 MeV-α) and ceramic (1500 ph/5.5 MeV-α) forms. Although γ-ray measurement requires further improvement in *LY* and crystallinity, it is realized that $(C_6H_5C_2H_4NH_3)_2PbI_4$ is a promising material as a fast-response scintillator owing to the quantum confinement effect.

Acknowledgments

This work was supported by Grants-in-Aid for Scientific Research, Scientific Research B (19H03533, 21H03733, and 21H03736), and Early-Career Scientists (20K20104 and 20K15026). The Cooperative Research Project of the Research Center for Biomedical Engineering, Nippon Sheet Glass Foundation, and SEI Group CSR Foundation are also acknowledged.

References

1 M. J. Weber: J. Lumin. **100** (2002) 35. https://doi.org/10.1016/S0022-2313(02)00423-4
2 T. Yanagida: Proc. Jpn. Acad., Ser. B **94** (2018) 75. https://doi.org/10.2183/pjab.94.007
3 S. E. Derenzo, E. Bourret-Courshesne, G. Bizarri, and A. Canning: Nucl. Instrum. Methods Phys. Res., Sect. A **805** (2016) 36. https://doi.org/10.1016/j.nima.2015.07.033

4 T. Yanagida, Y. Fujimoto, H. Masai, G. Okada, T. Kato, D. Nakauchi, and N. Kawaguchi: Sens. Mater. **33** (2021) 2179. https://doi.org/10.18494/SAM.2021.3315
5 H. Fukushima, M. Akatsuka, H. Kimura, D. Onoda, D. Shiratori, D. Nakauchi, T. Kato, N. Kawaguchi, and T. Yanagida: Sens. Mater. **33** (2021) 2235. https://doi.org/10.18494/SAM.2021.3324
6 D. Nakauchi, T. Kato, N. Kawaguchi, and T. Yanagida: Sens. Mater. **33** (2021) 2203. https://doi.org/10.18494/SAM.2021.3323
7 P. Lecoq: Nucl. Instrum. Methods Phys. Res., Sect. A **809** (2016) 130. https://doi.org/10.1016/j.nima.2015.08.041
8 Q. Wang, X. Tuo, C. Deng, L. Liu, Y. Cheng, C. Zhang, and Y. Yang: Nucl. Instrum. Methods Phys. Res., Sect. A **942** (2019) 162339. https://doi.org/10.1016/j.nima.2019.162339
9 W. W. Moses: Nucl. Instrum. Methods Phys. Res., Sect. A **487** (2002) 123. https://doi.org/10.1016/S0168-9002(02)00955-5
10 V. D. Ryzhikov, A. D. Opolonin, P. V. Pashko, V. M. Svishch, V. G. Volkov, E. K. Lysetskaya, D. N. Kozin, and C. Smith: Nucl. Instrum. Methods Phys. Res., Sect. A **537** (2005) 424. https://doi.org/10.1016/j.nima.2004.08.056
11 C. L. Melcher: J. Nucl. Med. **41** (2000) 1051. http://jnm.snmjournals.org/content/41/6/1051.abstract
12 K. Okazaki, D. Onoda, H. Fukushima, D. Nakauchi, T. Kato, N. Kawaguchi, and T. Yanagida: J. Mater. Sci.: Mater. Electron. **32** (2021) 21677. https://doi.org/10.1007/s10854-021-06686-9
13 P. Kantuptim, M. Akatsuka, D. Nakauchi, T. Kato, N. Kawaguchi, and T. Yanagida: Sens. Mater. **32** (2020) 1357. https://doi.org/10.18494/SAM.2020.2726
14 S. Surti: J. Nucl. Med. **56** (2015) 98. https://doi.org/10.2967/jnumed.114.145029
15 S. Surti and J. S. Karp: Physica Med. **32** (2016) 12. https://doi.org/10.1016/j.ejmp.2015.12.007
16 W. A. Berg, I. N. Weinberg, D. Narayanan, M. E. Lobrano, E. Ross, L. Amodei, L. Tafra, L. P. Adler, J. Uddo, W. Stein, and E. A. Levine: Breast J. **12** (2006) 309. https://doi.org/10.1111/j.1075-122X.2006.00269.x
17 K. Shibuya, M. Koshimizu, Y. Takeoka, and K. Asai: Nucl. Instrum. Methods Phys. Res., Sect. B **194** (2002) 207. https://doi.org/10.1016/S0168-583X(02)00671-7
18 A. Horimoto, N. Kawano, D. Nakauchi, H. Kimura, M. Akatsuka, and T. Yanagida: Sens. Mater. **32** (2020) 1395. https://doi.org/10.18494/SAM.2020.2747
19 M. Koshimizu, N. Kawano, A. Kimura, S. Kurashima, M. Taguchi, Y. Fujimoto, and K. Asai: Sens. Mater. **33** (2021) 2137. https://doi.org/10.18494/SAM.2021.3314
20 N. Imanaka, M. Hiraiwa, S. Tamura, G. Adachi, H. Dabkowska, and A. Dabkowski: J. Cryst. Growth **200** (1999) 169. https://doi.org/10.1016/S0022-0248(98)01407-9
21 D. Nakauchi, T. Kato, N. Kawaguchi, and T. Yanagida: Sens. Mater. **32** (2020) 1389. https://doi.org/10.18494/SAM.2020.2751
22 M. Akatsuka, D. Nakauchi, T. Kato, N. Kawaguchi, and T. Yanagida: Sens. Mater. **32** (2020) 1373. https://doi.org/10.18494/SAM.2020.2743
23 N. Kawano, M. Koshimizu, G. Okada, Y. Fujimoto, N. Kawaguchi, T. Yanagida, and K. Asai: Sci. Rep. **7** (2017) 14754. https://doi.org/10.1038/s41598-017-15268-x
24 N. Kawano, A. Horimoto, H. Kimura, D. Nakauchi, M. Akatsuka, and T. Yanagida: Mater. Res. Bull. **142** (2021) 111409. https://doi.org/10.1016/j.materresbull.2021.111409
25 M. Akatsuka, N. Kawano, T. Kato, D. Nakauchi, G. Okada, N. Kawaguchi, and T. Yanagida: Nucl. Instrum. Methods Phys. Res., Sect. A **954** (2020) 161372. https://doi.org/10.1016/j.nima.2018.10.050
26 D. Onoda, M. Akatsuka, N. Kawano, D. Nakauchi, T. Kato, N. Kawaguchi, and T. Yanagida: Opt. Mater. **114** (2021) 111002. https://doi.org/10.1016/j.optmat.2021.111002
27 D. Onoda, M. Akatsuka, N. Kawano, D. Nakauchi, T. Kato, N. Kawaguchi, and T. Yanagida: J. Lumin. **237** (2021) 118157. https://doi.org/10.1016/j.jlumin.2021.118157
28 D. Nakauchi, N. Kawano, N. Kawaguchi, and T. Yanagida: Jpn. J. Appl. Phys. **59** (2020) SCCB04. https://doi.org/10.7567/1347-4065/ab515d
29 K. Shibuya, M. Koshimizu, H. Murakami, Y. Muroya, Y. Katsumura, and K. Asai: Jpn. J. Appl. Phys. **43** (2004) L1333. https://doi.org/10.1143/JJAP.43.L1333
30 T. Yanagida, K. Kamada, Y. Fujimoto, H. Yagi, and T. Yanagitani: Opt. Mater. **35** (2013) 2480. https://doi.org/10.1016/j.optmat.2013.07.002
31 T. Yanagida, Y. Fujimoto, T. Ito, K. Uchiyama, and K. Mori: Appl. Phys. Express **7** (2014) 062401. https://doi.org/10.7567/APEX.7.062401
32 J. Yang, Y. Yu, L. Zeng, Y. Li, Y. Pang, F. Huang, and B.-L. Lin: J. Nanomater. **2017** (2017) 1. https://doi.org/10.1155/2017/1640965
33 M. Hu, Z. Liu, Q. Meng, and Q. Dong: Proc. Int. Conf. Optoelectronics and Measurement (2020) 208. https://doi.org/10.1007/978-981-13-8595-7_27

34 S. Zhang, P. Audebert, Y. Wei, A. Al Choueiry, G. Lanty, A. Bréhier, L. Galmiche, G. Clavier, C. Boissière, J.-S. Lauret, and E. Deleporte: Materials **3** (2010) 3385. https://doi.org/10.3390/ma3053385
35 T. Ishihara: J. Lumin. **60**–**61** (1994) 269. https://doi.org/10.1016/0022-2313(94)90145-7
36 J. Yu, J. Kong, W. Hao, X. Guo, H. He, W. R. Leow, Z. Liu, P. Cai, G. Qian, S. Li, X. Chen, and X. Chen: Adv. Mater. **31** (2018) 1806385. https://doi.org/10.1002/adma.201806385
37 N. Kitazawa, M. Aono, and Y. Watanabe: Mater. Chem. Phys. **134** (2012) 875. https://doi.org/10.1016/j.matchemphys.2012.03.083
38 K. Tanaka and T. Kondo: Sci. Technol. Adv. Mater. **4** (2003) 599. https://doi.org/10.1016/j.stam.2003.09.019
39 M. D. Birowosuto, D. Cortecchia, W. Drozdowski, K. Brylew, W. Lachmanski, A. Bruno, and C. Soci: Sci. Rep. **6** (2016) 37254. https://doi.org/10.1038/srep37254
40 D. Onoda, M. Akatsuka, N. Kawano, D. Nakauchi, T. Kato, N. Kawaguchi, and T. Yanagida: Opt. Mater. **114** (2021) 111002. https://doi.org/10.1016/j.optmat.2021.111002
41 K. Shibuya, M. Koshimizu, K. Asai, and H. Shibata: Appl. Phys. Lett. **84** (2004) 4370. https://doi.org/10.1063/1.1756203
42 D. Onoda, M. Akatsuka, N. Kawano, D. Nakauchi, T. Kato, N. Kawaguchi, and T. Yanagida: J. Mater. Sci.: Mater. Electron. **31** (2020) 20798. https://doi.org/10.1007/s10854-020-04592-0
43 T. Yanagida, H. Takahashi, T. Ito, D. Kasama, T. Enoto, M. Sato, S. Hirakuri, M. Kokubun, K. Makishima, T. Yanagitani, H. Yagi, T. Shigeta, and T. Ito: IEEE Trans. Nucl. Sci. **52** (2005) 1836. https://doi.org/10.1109/TNS.2005.856757
44 T. Yanagida, Y. Fujimoto, K. Yamanoi, M. Kano, A. Wakamiya, S. Kurosawa, and N. Sarukura: Phys. Status Solidi C **9** (2012) 2284. https://doi.org/10.1002/pssc.201200176
45 K. Watanabe, M. Koshimizu, Y. Fujimoto, Y. Hayashi, H. Takizawa, T. Yanagida, and K. Asai: Radiat. Meas. **106** (2017) 146. https://doi.org/10.1016/j.radmeas.2016.12.007
46 D. Nakauchi, T. Kato, N. Kawaguchi, and T. Yanagida: Appl. Phys. Express **13** (2020) 122001. https://doi.org/10.35848/1882-0786/abc574